INAF
ISTITUTO NAZIONALE
DI ASTROFISICA
NATIONAL INSTITUTE
FOR ASTROPHYSICS



| | |
|---|---|
| ***Publication Year*** | 2022 |
| ***Acceptance in OA*** | 2025-03-19T11:22:40Z |
| ***Title*** | Red giant branch bump brightness in 7 metal-poor globular clusters obtained with GAIA DR2 |
| ***Authors*** | Song, Fen, Yuan, Zunli, Li, Yan, Wu, Xuchao, PIETRINFERNI, Adriano, Poon, Helen, Wu, Tao, Nie, Jundan, Song, Hanfeng, Han, Cheng, Yang, Ye, Li, Yuxuan, Bai, Xingming |
| ***Publisher's version (DOI)*** | 10.1007/s10509-022-04058-1 |
| ***Handle*** | http://hdl.handle.net/20.500.12386/36870 |
| ***Journal*** | ASTROPHYSICS AND SPACE SCIENCE |
| ***Volume*** | 367 |

Astrophysics and Space Science (2022) 367:32
https://doi.org/10.1007/s10509-022-04058-1

ORIGINAL ARTICLE

# Red giant branch bump brightness in 7 metal-poor globular clusters obtained with GAIA DR2

Fen Song[1,2] · Zunli Yuan[3] · Yan Li[2,4,5,6] · Xuchao Wu[1] · Adriano Pietrinferni[7] · Helen Poon[8] · Tao Wu[4] · Jundan Nie[9] · Hanfeng Song[2,10,11] · Cheng Han[1] · Ye Yang[1] · Yuxuan Li[1] · Xingming Bai[1]

Received: 9 August 2021 / Accepted: 23 February 2022 / Published online: 15 March 2022
© The Author(s), under exclusive licence to Springer Nature B.V. 2022

**Abstract**
The identification of the red giant branch bump brightness in metal-poor globular clusters is important for low-mass stellar evolution. The release of *Gaia* DR2 prompted us to revisit the red giant branch bump (RGBB) in galactic globular clusters. We apply a popular nonparametric density estimation approach, kernel density estimation (KDE), to explore the position of RGBB in 7 metal-poor globular clusters (GCs). The $G$ and $V$ magnitudes of the RGBB according to our clustering algorithm, $G_{B,K}$ and $V_{B,K}$, respectively show the RGB bump magnitude detected by the KDE method in $G$ band and $V$ band. They show the overdensity location in the luminosity function of the RGB stars. Based on the results derived by KDE, a maximum-likelihood analysis via a Markov Chain Monte Carlo (MCMC) approach is adopted to detect the RGB bump feature and obtain more accurate RGBB brightnesses in $G$ band and $V$ band for the samples. We find that the red giant branch bump brightness becomes fainter as the global metallicity increases in clusters with [M/H] $\leq -1.4$. We present the empirical relation between the global metallicity [M/H] and absolute magnitude $M_V$ of the red giant branch bump for clusters with [M/H] $\leq -1.4$. We verify that discrepancies between observations and theory for metal-poor globular clusters with [M/H] $\leq -1.4$.

**Keywords** Globular clusters: general · Red giant branch bump · Hertzsprung-Russell diagrams

## 1 Introduction

The red giant branch bump (RGBB) is an important evolutionary feature of a low-mass star before the helium flash. It is also an important feature in the colour magnitude diagrams (CMDs) of galactic globular clusters (abbreviated as GGCs). An RGBB is generated because the Hydrogen-burning shell encounters the chemical discontinuity caused by the first dredge-up in low-mass stars. The RGBB offers a direct test of what is going on in low-mass stars in the region where $T \sim 10^6$ K (Fusi Pecci et al. 1990). This provides us

✉ F. Song
fsong@jmu.edu.cn

Z. Yuan
yzl@hunnu.edu.cn

1 College of Science, Jimei University, Xiamen 361021, China

2 Key Laboratory for Structure and Evolution of Celestial Objects, Chinese Academy of Sciences, P.O. Box 110, Kunming 650216, China

3 Department of Physics, School of Physics and Electronics, Hunan Normal University, Changsha 410081, China

4 Yunnan Observatories, Chinese Academy of Sciences, P.O. Box 110, Kunming 650216, China

5 Center for Astronomical Mega-Science, Chinese Academy of Sciences, Beijing, 100012, China

6 University of Chinese Academy of Sciences, Beijing 100049, China

7 INAF-Osservatorio Astronomico d'Abruzzo, via M. Maggini, 64100 Teramo, Italy

8 Department of Physical Science, Hiroshima University, 1-3-1 Kagamiyama, Higashi-Hiroshima, Hiroshima 7398526, Japan

9 Key Laboratory of Optical Astronomy, National Astronomical Observatories, Chinese Academy of Sciences, Beijing 100012, China

10 College of Physics, Guizhou University, Guiyang, Guizhou Province, 550025, China

11 Geneva Observatory, Geneva University, 1290 Sauverny, Switzerland

with information about the chemical profile above the H-burning shell inside red giant stars and mixing processes in low-mass stars (Cassisi et al. 2002). Therefore, it serves as a direct test of assumptions of stellar evolution.

After the work of King et al. (1985) in Cluster 47 Tuc, astronomers found that the number of stars occupying the RGBB is 2-3 times larger than those adjacent to the RGBB in the RG branch. The RGB bump appears as a change in the slope of the cumulative luminosity function (CLF) and appears as a peak in the differential luminosity function (DLF). The DLF and CLF have been used to find the RGBB features of globular clusters by astronomers for a long time (Fusi Pecci et al. (1990), Zoccali et al. (1999), Ferraro et al. (1999), Riello et al. (2003)). Until now, differential and cumulative luminosity functions have been important methods to detect the RGB bump feature and obtain the RGBB magnitude. Therefore, the DLF is used to derive the RGBB magnitude of metal-poor globular clusters to verify the results presented by KDE and the maximum-likelihood analysis in this work.

A few metal-poor GGCs have been discussed in previous works (Alves and Sarajedini 1999; Bono et al. 2001; Di Cecco et al. 2010; Cassisi et al. 2011; Nataf et al. 2013; Nataf 2014; Cohen et al. 2015; Joyce and Chaboyer 2015). Many studies comparing theory and observations of RGBB magnitudes in globular clusters (GCs) have been presented (Fusi Pecci et al. 1990; Cassisi and Salaris 1997; Riello et al. 2003; Bjork and Chaboyer 2006; Di Cecco et al. 2010; Joyce and Chaboyer 2015; Song et al. 2018). Discrepancies between theory and observations in the RGBB brightnesses of metal-poor clusters with $[Fe/H] \leqslant -1.5$ have been found (Di Cecco et al. 2010; Joyce and Chaboyer 2015). Thus, the more accurate RGBB magnitude identified by observational data is useful for astrophysicists to provide limits for stellar evolution and the galaxy because metal-poor globular clusters are one of the oldest known objects in the galaxy.

The field of view in *Gaia* is all-sky. Thus the *Gaia* Data can include all of the stars in the cluster. *Gaia* can obtain the larger stellar samples than the HST samples (Piotto et al. 2002; Sarajedini et al. 2007), particularly for clusters for which the half-light radius is comparable to or greater than the HST field of view of approximately 2 arcminutes. When we use *Gaia* DR2 to investigate metal-poor globular clusters, we would have a larger number counts for clusters, and thus have better statistics. In addition, the significant field contamination of globular clusters can be cleaned with a proper motion criterion. In the work, we use *Gaia* DR2 to revisit the metal-poor globular clusters. We test a new technique on up-to-date to obtain the RGBB magnitudes and improve data. Seven metal-poor galactic globular clusters with $[M/H] \leqslant -1.4$ are chosen in our work. The identifications of the RGBB in 7 GGCs are presented.

Kernel density estimation (KDE) is a well-established nonparametric approach to estimate continuous density functions (Yuan et al. 2020). Due to its effectiveness and flexibility, it has become an important tool for analysing data. To the best of our knowledge, this is the first work to use KDE to detect the RGB bump feature and obtain the RGB bump brightness. To verify the results, a maximum-likelihood analysis via the Markov Chain Monte Carlo (MCMC) approach presented by Nataf et al. (2013) and the differential Luminosity Function (DLF) are also adopted to detect the RGBB features of metal-poor globular clusters.

First, the colour-magnitude diagrams of 7 metal-poor globular clusters are obtained and shown in Sect. 2. The RGB bump brightnesses of 7 metal-poor GGCs are obtained by implementing KDE, the maximum-likelihood analysis and the DLF in Sect. 3. Section 4 shows the relation between metallicity and RGBB brightnesses for metal-poor GCs with $[M/H] \leqslant -1.4$. A comparison between theory and observation is presented in Sect. 5. Discussion is presented in the last Section.

## 2 Colour-magnitude diagrams

The second *Gaia* photometric catalogue (*Gaia* DR2) has been released in April 2018 (Gaia Collaboration et al. 2018b). The latest G-band photometry (330 nm-1050 nm) for approximately 1.7 billion sources and $G_{BP}$ (330 nm-680 nm) and $G_{RP}$ (630 nm-1050 nm) photometry of 80% of them are presented in the *Gaia* DR2 (Evans et al. 2018). Positions, parallaxes, and proper motions of sources with $G \leqslant 21$ mag have been presented (Gaia Collaboration et al. 2018b,d). Gaia Collaboration et al. (2018d) determined the proper motions of galactic globular clusters and identified member stars of GCs. Gaia Collaboration et al. (2018d) took into account the ability of distinguishing (in Proper motion and parallax space) the cluster stars from those in the field, both as a function of distance from the cluster centre and of magnitude. Then they obtained data of 75 GGCs. According to the member stars of GCs identified by Gaia Collaboration et al. (2018d), we obtained colour-magnitude diagrams (CMDs) of 75 GGCs based on photometric data of *Gaia* DR2 (Gaia Collaboration et al. 2016, 2018b). We chose 7 metal-poor globular clusters with $[M/H] \leq -1.4$ from their samples.

Seven metal-poor galactic globular clusters with $[M/H] \leq -1.4$ are presented in our work. The feature of the RGB bump is identified in galactic globular clusters NGC 4590, NGC 5139, NGC 5466, NGC 5897, NGC 6397, NGC 6656 and NGC 6809. These GCs are all among the most metal-poor globular clusters in the catalogue presented by Harris (2010). NGC 5466 has the lowest-metallicity in the catalogue except for NGC 7078. The metallicities of GCs in our database are presented in Table 1. The interstellar reddening is also listed in Table 1. All samples have low-reddening

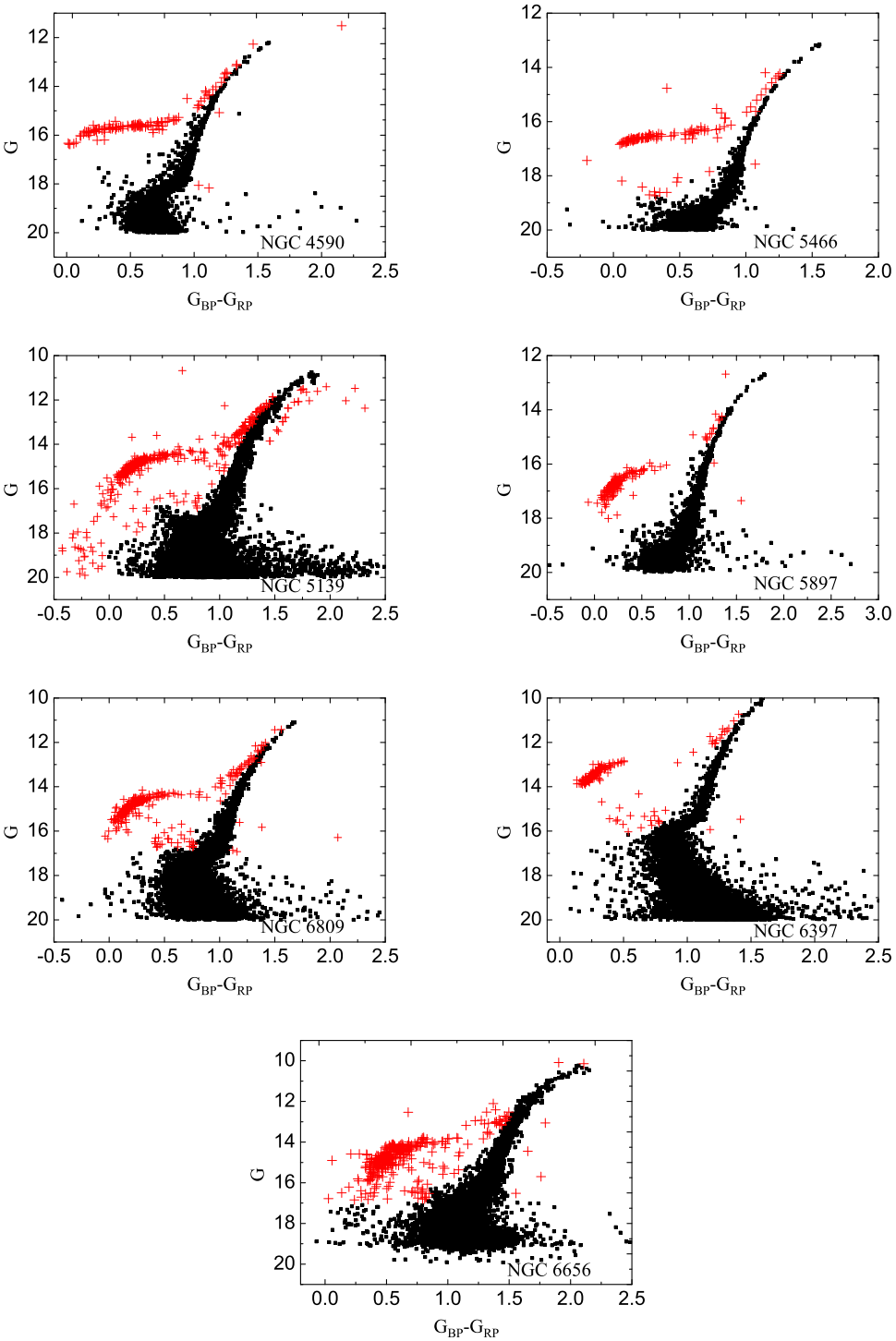


**Fig. 1** Colour-magnitude diagrams of 7 metal-poor galactic globular clusters, employing photometric data of *Gaia* DR2. Black squares indicate the restricted zone. Red pluses are stars exceeding the restricted zone. The width of the limited zone in $G_{BP} - G_{RP}$ is estimated. Red pluses show the deleted points from CMDs. Black squares in the RGB are used to detect RGBB features in each cluster

($E(B-V) \leq 0.26$). The RGBB brightness in 7 samples was presented by Fusi Pecci et al. (1990), Sarajedini (1992), Ferraro et al. (1999), Riello et al. (2003), Sollima et al. (2005), Fekadu et al. (2007), and Nataf et al. (2013). The most well-studied, metal-poor GGCs, are revisited with the nonparametric method (KDE), maximum-likelihood analysis and differential luminosity function.

The CMDs of 7 metal-poor GCs obtained with *Gaia* DR2 are shown in Fig. 1. In Fig. 1, black squares in the RGB are used to detect RGBB features and derive RGBB magnitude. Black squares are chosen in the restricted zone at the brighter portion of the RGB, because the identifications of the RGBB in each cluster will be affected by a poor colour separation between RGB stars and AGB stars, especially at

**Table 1** The parameters of 7 metal-poor GGCs

| Name | $E(B-V)$[a] | [Fe/H] | [$\alpha$/Fe] | [M/H] |
|---|---|---|---|---|
| NGC 4590 | 0.05[1] | $-2.27 \pm 0.04$ | 0.31 | $-2.05$ |
| NGC 5139 | 0.12[1] | $-1.64 \pm 0.09$ | 0.30 | $-1.43$ |
| NGC 5466 | 0.00[1] | $-2.31 \pm 0.09$ | 0.39 | $-2.02$ |
| NGC 5897 | 0.09[1] | $-1.90 \pm 0.06$ | 0.34 | $-1.66$ |
| NGC 6397 | 0.18[1] | $-1.99 \pm 0.02$ | 0.4 | $-1.70$ |
| NGC 6809 | 0.08[1] | $-1.93 \pm 0.02$ | 0.41 | $-1.63$ |
| NGC 6656 | 0.34[1] | $-1.70 \pm 0.08$[b] | – | $-1.42$[b] |

*Note*: $E(B-V)$, [Fe/H], [$\alpha$/Fe] and [M/H] respectively present the reddening, metal metallicity, $\alpha$-enhanced abundance and the global metallicity in each cluster

[a] $E(B-V)$ is presented by Harris (2010)

[b] Nataf et al. (2013)

the brightest portion of the RGB. Red pluses are stars exceeding the restricted zone. We identified most red pluses as stars in the asymptotic giant branch (AGB) and horizontal branch (HB) strictly by eye. Therefore, red pluses are deleted from the *Gaia* data to obtain more precise results. The CMDs shown in Fig. 1 for some GCs look much poorer than many obtained with HST. However, this is the first in a series of papers devoted to studies of RGBB in metal-poor GCs using *Gaia* DR2 data. And *Gaia* data have better statistics due to its field of view. Unfortunately, although Piotto et al. (2015) found that all the GCs host multiple stellar populations obtained with the UV Legacy survey of GCs, the *Gaia* photometric filters are not sensitive to the specific chemical composition of GCs. Thus, these samples all serve as a single population in CMDs.

## 3 The RGBB brightnesses of metal-poor globular clusters in galaxy derived by KDE and maximum-likelihood analysis

### 3.1 Kernel density estimation

KDE is the most popular nonparametric density estimation approach developed in modern statistics. Due to its effectiveness and flexibility, it has gradually been recognized by the astronomical community as a powerful tool to analyse data (e.g., Hatfield et al. 2016; Yuan et al. 2018, 2020). To our knowledge, we are the first to use KDE to explore the location of the RGBB based on observational data.

Let $\{X_1, X_2, \ldots, X_n)\}$ be a univariate independent sample drawn from some distribution with an unknown density $f(x)$. The KDE to $f$ can be given by

$$f(x) = \frac{1}{nh}\sum_{j=1}^{n} K\left(\frac{x - X_j}{h}\right), \tag{1}$$

where $K$ is the kernel function and $h$ is a smoothing parameter called the bandwidth (e.g., Gramacki 2018). The choice of kernel function is not critical (e.g., Botev et al. 2010; Gramacki 2018) and usually the normal kernel is used, i.e., $K(x)$ is taken as the standard normal density function (e.g., Yuan et al. 2018, 2020). The critical issue in using KDE is to choose an optimal $h$. In addition, Equation (1) implicitly assumes that the domain of the data is unbounded. However, obviously, the observed data (G-band magnitudes) in this work are bounded. Using Equation (1) on bounded data can cause certain deficiencies known as boundary bias (see Gramacki 2018; Yuan et al. 2020, for detail). We follow the method of Botev et al. (2010) to overcome the boundary bias problem and choose an optimal $h$. The KDE results here are calculated by the MATLAB program "Kernel Density Estimator for One-dimensional Data" provided by Botev et al. (2010).

In Fig. 2, the red solid line shows the density distribution of the RGB stars derived by KDE. The overdensity position in the luminosity function of RGB shows the RGB bump. The RGBB magnitude, $G_{B,K}$, is obtained according to the overdensity position and is presented in Table 2. The RGBB magnitude, $G_{B,K}$, is used to restrict the explored space of parameter $G_{B,M}$ in the maximum-likelihood analysis.

### 3.2 The maximum-likelihood analysis

Nataf et al. (2013) presented a maximum-likelihood analysis via a Markov Chain Monte Carlo approach to obtain the RGBB brightness of GCs. Following the method of Nataf et al. (2013), a maximum-likelihood analysis via MCMC is carried out for 7 metal-poor globular clusters. Nataf et al. (2013) used an exponential function and a normal distribution to fit the luminosity function of RGB stars and RGBB stars, respectively. The parametric luminosity functions of the RGB and RGBB stars are also adopted in this work. $N(G)$ presents the luminosity function of the RGB and RGBB stars. It is presented in function (2). The exponential function shows the magnitude distribution of the red giant branch. The normal distribution shows the magnitude distribution of the red giant branch bump.

The integral of $N(G)$ over the magnitude range is the number of RGB star $N_{obs}$ of a globular cluster.

$$N(G) = Ae^{[B(G-G_{B,M})]} + \frac{N_B}{\sqrt{2\pi}\sigma_B} e^{-\frac{(G-G_{B,M})^2}{2\sigma_B^2}} \tag{2}$$

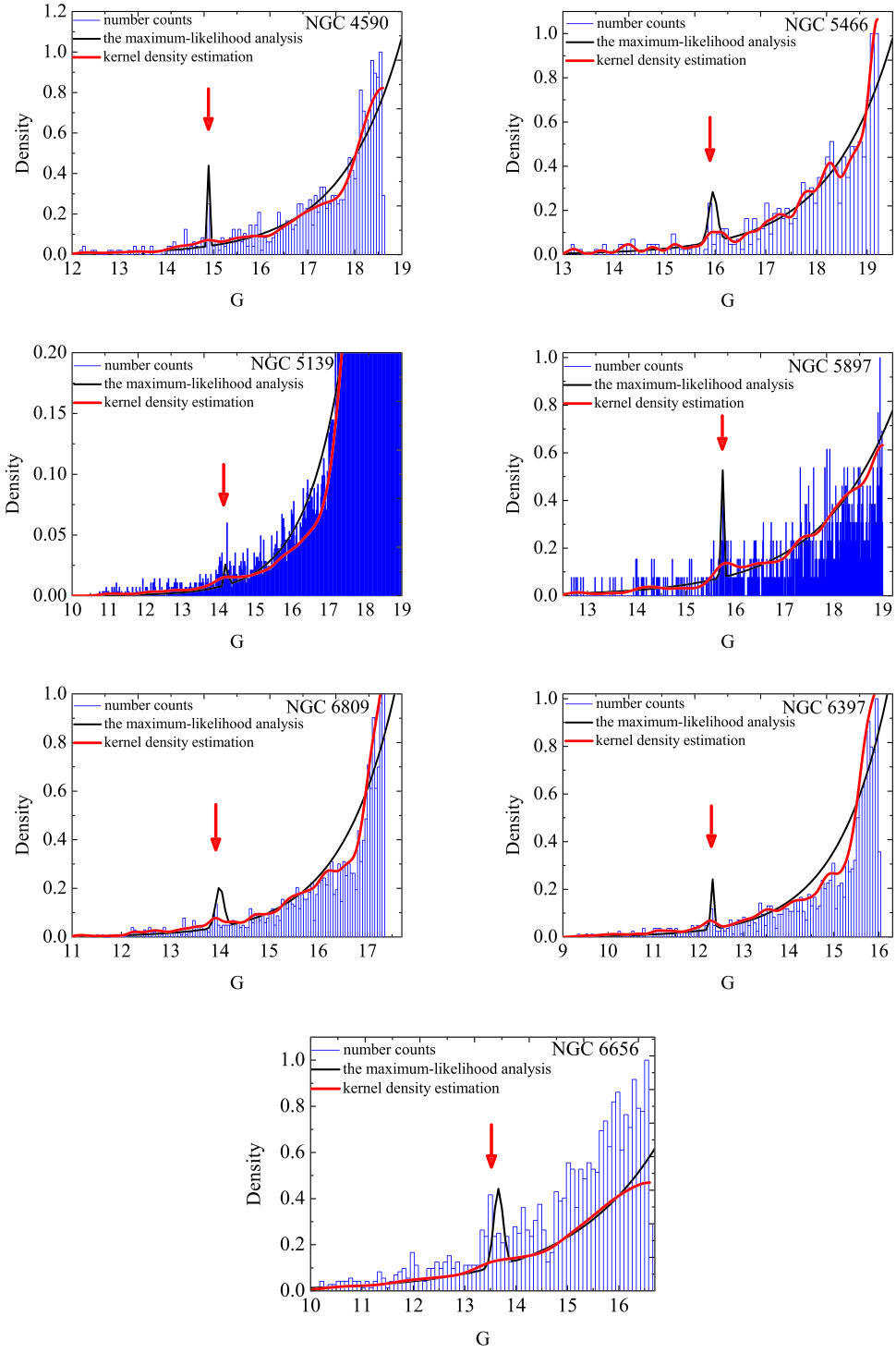


**Fig. 2** Histogram diagrams showing the normalized differential luminosity function (magnitude distributions) for the RGB in 7 metal-poor galactic globular clusters. The number of red giant stars on the RGBB is 2 times larger than those adjacent to the RGBB in RGB. The black solid curves indicate the normalized density function derived by the maximum-likelihood analysis via MCMC. The red solid curves show the density distribution of the RGB stars derived by KDE. The red arrows indicate the location of the detected RGBB

$$N(G) = A\{e^{[B(G-G_{B,M})]} + \frac{EW_B}{\sqrt{2\pi}\sigma_B} e^{-\frac{(G-G_{B,M})^2}{2\sigma_B^2}}\} \quad (3)$$

$G_{B,M}$ is the average brightness of the RGB bump in the G band. $A$ defines the total normalization of the population. It is determined through the integral of $N(G)$ over the magnitude range of the red giant branch based on function (2). $B$ describes an exponential luminosity function of the RG branch. $EW_B$ is calculated by $\frac{N_B}{A}$, and $N_B$ is the number of stars on the RGBB. The integral of the normal distribution over the red giant branch bump is the number of RGBB star $N_B$. The luminosity dispersion of the RGBB is described by $\sigma_B$.

The likelihood function $p(G_{obs}|\theta)$ for the observed data can be derived, once we have a parametric form for $N(G)$,

with parameters $\theta$. Nataf et al. (2013) gave a log-likelihood function $S$, i.e., $S \equiv -2\ln(p(G_{obs}|\theta))$, and

$$S = -2\left\{\sum_{i}^{N_{obs}} \ln\left[N\left(G_i, A, B, EW_B, \sigma_B, G_{B,M}\right)\right] - N_{obs}\right\}. \tag{4}$$

To perform a Bayesian analysis, one needs to write down the posterior probability function:

$$p(\theta|G_{obs}) \propto p(\theta)p(G_{obs}|\theta) \tag{5}$$

where $p(G_{obs}|\theta)$ is the observed data likelihood function defined in Equation (4), and $p(\theta)$ is the prior distribution of $\theta$, which should convey information known prior to the analysis (Yuan et al. 2016). In this work, we assume a uniform prior on parameters. This is equivalent to setting value ranges for them. According to Equation (5), we can draw parameter samples using the MCMC Algorithm. The MCMC sampler used here is the public code "COSMOMC" of Lewis and Bridle (2002). Specifically, the explored parameter space of $\sigma_B$ and $B$ in the log-likelihood function are restricted in the following range:

$$0.001 \leqslant \sigma_B \leqslant 0.1, 0.0 \leqslant B \leqslant 1.0. \tag{6}$$

The explored parameter space of $G_{B,M}$ has an important influence on finding the location of the RGBB during the maximum-likelihood analysis. The explored parametric space of $G_{B,M}$ is determined by the parameter $G_{B,K}$. The RGB bump brightness $G_{B,K}$ is obtained by kernel density estimation based on the observed RGB data. The explored parametric space of $G_{B,M}$ is limited as follows (7):

$$\left|G_{B,M} - G_{B,K}\right| \leqslant 0.5 \tag{7}$$

In Fig. 2, the black solid line represents the normalized density distribution in the red giant branch. The normal distribution fits the luminosity function of the RGB bump stars. The location of the Gaussian peak shows the RGBB magnitude. $G_{B,M}$ is presented in Table 2. The best-fit values of the parameters in the model are shown in Table 2.

### 3.3 The differential luminosity function

King et al. (1985) derived the luminosity function for the red giant branch in 47 Tuc. The differential luminosity function (DLF) is obtained by counting the number of stars in 0.1 mag bins wide in V for the RGB. The peak in the magnitude range indicates that the hydrogen-burning shell in a red giant branch star encounters the composition discontinuity. The feature of the red giant branch bump is found and presented. Following the work of King et al. (1985), we also use the differential luminosity function to search the RGBB in all samples. Then, the results are compared with the RGBB magnitudes presented by KDE and the maximum-likelihood analysis.

In Fig. 1, black squares in the RGB in each clusters are used to obtain magnitude distributions of the red giant branch stars by adopting the DLF. The normalized DLFs of the red giant stars (the normalized magnitude distributions) for 7 globular clusters are shown in Fig. 2. In Fig. 2, the red arrows indicate the location of detected RGBB by the differential luminosity function. The values of $G_{B,D}$ of 7 GGCs are given in Table 2. The associated error of $G_{B,D}$ is presented by $\delta$ in Table 2. The parameter $\delta$ is presented as $\sigma/\sqrt{(N-1)}$, $\sigma$ is the 68.26th percentile of the absolute deviation from the mean $G$ distribution, and $N$ is the number of stars located on the RGBB.

We require that the number of red giant stars on the identified RGBB is 2 times larger than those adjacent to the RGBB in the RGB for each cluster (King et al. 1985). By adjusting the bins, the feature of the RGB bump in our samples can be found. The results are presented in Table 2 and shown in Fig. 2. The RGB bump magnitudes are consistent with the results obtained by KDE and the maximum-likelihood analysis. However, the RGBB magnitudes presented by KDE and the maximum-likelihood analysis are independent of the bin.

### 3.4 Comparisons with other results

To compare with the previous results presented by other works, the magnitude $G$ of the red giant branch stars is transformed to $V$ by using the Carrasco colour-transformation relations presented by Carrasco et al. (2016) and Evans et al. (2018). The photometric transformation between *Gaia* DR2 and Johnson-Cousins (Landolt (2009)) is presented in Equation (8). In function (8), $G$, $G_{BP}$ and $G_{RP}$ show magnitudes in *Gaia* passbands. $V$ shows magnitude in Johnson-Cousins passband. The function (8) is fitted by polynomials. The associated error in the transformed $V$ is 0.045858 mag. The range of applicability for the colour-transformation relationship into the Johnson-Cousins band is $-0.5 < G_{BP} - G_{RP} < 2.75$. To limit the influence of the photometric noise in the derived relationship (function (8)), *Gaia* DR2 sources were cross-matched with $G < 13$ mag. The chosen 398 sources with small magnitude errors and small excess fluxes were used for the fitting. The additional uncertainties from the relationship will be included in the magnitude $V$.

$$\begin{aligned} G - V = &[-0.0176 - 0.00686(G_{BP} - G_{RP}) \\ &-0.1732(G_{BP} - G_{RP})^2] \end{aligned} \tag{8}$$

Based on the transformed magnitudes in $V$ band, KDE is used to explore the RGB bump features of clusters.

**Table 2** The RGB bump brightnesses of 7 metal-poor GGCs based on the data of *Gaia* DR2

| Name | | $G_{B,D} \mp \delta$ | $G_{B,K} \mp \sigma_K$ | $G_{B,M}$ | $B$ | $\sigma_B$ | $V_{B,K}$ | $V_{B,M}$ | $\sigma_{B,V}$ | $V_{bump}^{Lit}$ |
|---|---|---|---|---|---|---|---|---|---|---|
| NGC 4590 | M 68 | $14.89 \mp 0.01$ | $14.90 \mp 0.21$ | 14.90 | $0.79^{-0.02}_{+0.02}$ | $0.019^{-0.002}_{+0.001}$ | 15.122 | $15.13^{-0.02}_{+0.01}$ | 0.044 | $15.149 \pm 0.011$ [2], $15.15 \pm 0.05$ [3] |
| NGC 5139 | $\omega$ Cen | $14.23 \mp 0.00$ | $14.15 \mp 0.89$ | 14.38 | $0.83^{-0.01}_{+0.01}$ | $0.089^{-0.001}_{+0.007}$ | 14.512 | $14.63^{-0.00}_{+0.01}$ | 0.098 | $14.31 \pm 0.03$, $14.42 \pm 0.03$, $14.57 \pm 0.03$, $14.84 \pm 0.04$[7] |
| NGC 5466 | | $15.90 \mp 0.01$ | $15.97 \mp 0.60$ | 15.96 | $0.80^{-0.03}_{+0.02}$ | $0.081^{-0.010}_{+0.000}$ | 16.182 | $16.30^{-0.00}_{+0.00}$ | 0.071 | $16.2 \pm 0.05$ [4] |
| NGC 5897 | | $15.76 \mp 0.00$ | $15.83 \mp 0.23$ | 15.74 | $0.67^{-0.02}_{+0.02}$ | $0.024^{-0.001}_{+0.001}$ | 16.038 | $16.05^{-0.01}_{+0.00}$ | 0.053 | $16.0 \pm 0.1$ [3], 16.0 [5] |
| NGC 6397 | | $12.29 \mp 0.01$ | $12.27 \mp 0.27$ | 12.31 | $0.88^{-0.03}_{+0.01}$ | $0.034^{-0.006}_{+0.000}$ | 12.589 | $12.62^{-0.01}_{+0.00}$ | 0.023 | $12.533 \pm 0.046$ [2], $12.6 \pm 0.1$ [6] |
| NGC 6809 | | $13.92 \mp 0.00$ | $13.92 \mp 0.16$ | 14.01 | $0.90^{-0.01}_{+0.01}$ | $0.081^{-0.004}_{+0.006}$ | 14.192 | $14.19^{-0.00}_{+0.00}$ | 0.025 | $14.151 \pm 0.013$ [2], $14.15 \pm 0.05$ [3] |
| NGC 6656 | M 22 | $13.50 \mp 0.04$ | $13.52 \mp 0.12$ | 13.65 | $0.57^{-0.01}_{+0.01}$ | $0.089^{-0.01}_{+0.00}$ | 13.936 | $13.75^{-0.00}_{+0.00}$ | 0.089 | $13.974 \pm 0.013$ [2], 13.91, 14.06 [8] |

*Note*: (1) $G_{B,D}$ and $\delta$ respectively show the RGBB magnitude and error of the RGBB magnitude detected by the DLFs. $G_{B,K}$ shows the RGBB magnitude in G band, which is derived by KDE. $G_{B,M}$ and $\sigma_B$ respectively present the RGBB magnitude in G band and its error confirmed by the maximum-likelihood analysis via MCMC. $B$ represent the parameter in an exponential luminosity function. $V_{B,K}$ represents the RGBB magnitude obtained by KDE. $V_{B,M}$ shows the RGBB magnitude in V, which is derived by the maximum-likelihood analysis based on the results of KDE. $\sigma_{B,V}$ shows the luminosity dispersion of the RGBB derived by the maximum-likelihood analysis. $V_{bump}^{Lit}$ shows the previous results for the RGBB in the same cluster, which is presented by other works listed in (2). (2) [1] Harris (2010); [2] Nataf et al. (2013); [3] Ferraro et al. (1999); [4] Fekadu et al. (2007); [5] Sarajedini (1992); [6] Fusi Pecci et al. (1990); [7] Sollima et al. (2005); [8] Lee (2015)

The RGB bump magnitude in $V$ derived by the KDE is showed by $V_{B,K}$ in Table 2. Based on the results derived by the KDE, the maximum-likelihood analysis presented in Sect. 3.1 is used to obtain the RGBB magnitudes. The log-likelihood function $S$ and $N(V)$ are as follows:

$$S = -2\left\{\sum_{i}^{N_{obs}} \ln\left[N\left(V_i, A, B, EW_B, \sigma_{B,V}, V_{B,M}\right)\right] - N_{obs}\right\} \tag{9}$$

$$N(V) = Ae^{[B(V-V_{B,M})]} + \frac{N_B}{\sqrt{2\pi}\sigma_{B,V}} e^{-\frac{(V-V_{B,M})^2}{2\sigma^2_{B,V}}} \tag{10}$$

where the parameter space is limited by:

$$\left|V_{B,M} - V_{B,K}\right| \leqslant 0.2 \tag{11}$$

$V_{B,K}$ and $V_{B,M}$ are all shown in Table 2. $V^{Lit}_{bump}$ represents the RGBB magnitudes obtained by the listed in Table 2. It shows the previous results presented by other researchers.

In NGC 4590, the location of the RGBB by the DLF is at 14.89 mag in the G band. Based on the determined parameter space, the obtained RGBB magnitude $G_{B,M}$ by the maximum-likelihood analysis is $14.90 \pm 0.02$ mag in G. After transforming into the V band, the RGBB magnitude in V is $15.13 \pm 0.04$ mag. Previous results can be found in Ferraro et al. (1999), Riello et al. (2003) and Nataf et al. (2013). Nataf et al. (2013) presented that the RGBB magnitudes in V are 15.149 mag with an error of 0.011 mag. Ferraro et al. (1999) used the cumulative luminosity function and found that the RGBB magnitude in V is 15.15 mag with an error of 0.05 mag. In the KDE, we found that the magnitude of the overdensity in the magnitude distribution of the RGB is 15.122 mag in $V$. Based on the KDE results, the maximum-likelihood analysis yields an RGBB magnitude of 15.13 mag. Our result is consistent with the results of Nataf et al. and Ferraro et al. However, the RGBB magnitude $V_{B,M}$ is 0.02 mag less than the results presented by Ferraro et al. (1999) and Nataf et al. (2013). Based on *Gaia* DR2, Perren et al. (2020) used the polynomial (Eq. (8)) to get the transformed $V_{Gaia}$ from $G$ band for open clusters in Mily Way. They estimated the systematic error between the transformed $V_{Gaia}$ and V-band photometry, and presented the mean differences $\sim 0.03$. Considering the systematic error, we find that the RGBB magnitudes $V_{B,K}$ and $V_{B,M}$ are consistent with results presented by Nataf et al. (2013) and Ferraro et al. (1999).

NGC 5139 is a peculiar cluster because of its metallicity spread (Sollima et al. (2005)). It is the most massive and luminous globular cluster in the Milky Way. According to the relationships presented by Nataf et al. (2013), the absolute magnitude of the RGBB in NGC 5139 is 0.36, whereas the absolute magnitude found in this work is 0.56. The apparent distance modulus is presented by Bellazzini et al. (2004). Pancino et al. (2000) reported on the discrete structure of the red giant branch of NGC 5139, based on the different metal abundance [Ca/H]. According to the stellar populations with different $\alpha$-element enhancement levels ([M/H]), Sollima et al. (2005) showed the five discrete populations of the RGB in NGC 5139. The RGB bump for each population appears as distinct peaks in the CMD. Sollima et al. (2005) noted that the RGBB magnitude of the metal-poor RGB with $[M/H] = -1.4 \pm 0.2$ is $14.31 \pm 0.03$ mag in V. They also obtained that the RGBB magnitudes of the metal-intermediate RGB with $[M/H] = -1.2 \pm 0.2$, $[M/H] = -0.9 \pm 0.2$, $[M/H] = -0.7 \pm 0.2$ were $14.42 \pm 0.03$ mag, $14.57 \pm 0.03$ mag and $14.84 \pm 0.04$ mag, respectively. Thus, according to the effect of a metallicity dispersion, four RGB bump magnitudes are detected by the differential luminosity functions in NGC 5139. We found that the RGB bump brightness of the metal-rich population is significantly fainter. The conclusion matches well with the result in NGC 6656 (M22) presented by Lee (2015).

A high and sharp peak appears in our density distribution. The magnitude of the peak is $14.63 \pm 0.098$ mag. This is in a range from 14.31 mag to 14.84 mag. The parameter $\sigma_{B,V}$ in the log-likelihood function is 0.098. The width of the RGBB ranges from $14.63 - 3\sigma_{B,V}$ mag to $14.63 + 3\sigma_{B,V}$ mag according to the normal distribution of the RGBB stars. The value of $14.63 - 3\sigma_{B,V}$ is 14.336, whereas $14.63 + 3\sigma_{B,V}$ is 14.924. Surprisingly, The value of $14.63 - 3\sigma_{B,V}$ is only 0.026 mag more than 14.31 mag, whereas $14.63 + 3\sigma_{B,V}$ is 0.08 mag more than 14.84 mag.

*Gaia* data are not sensitive to the element abundance. Therefore, we cannot analyse the RGBB of different populations of the RGB. However, to an extent, our result is consistent with the result presented by Sollima et al. (2005). The result of $0.36 \pm 0.01$ based on the relationships presented by Nataf et al. (2013) matches the result of Sollima et al. (2005) of 14.31 mag ($0.37 \pm 0.03$).

In NGC 5466, Fekadu et al. (2007) found that a small peak appeared in the differential luminosity function at $V = 16.2 \pm 0.05$ mag. Considering the systematic error, the RGB bump magnitude obtained by the KDE is $16.182 \pm 0.030$ mag. However, the RGBB magnitude 16.30 mag detected by the maximum-likelihood analysis is 0.1 mag larger than the result presented by Fekadu et al. (2007). The $\sigma_{B,V}$ in function (10) is 0.071. The width of the RGBB ranges from $16.30 - 3\sigma_{B,V}$ (16.09) mag to $16.30 + 3\sigma_{B,V}$ (16.51) mag. The results are consistent with the results presented by Fekadu et al. (2007).

Compared with the previous results presented on NGC 5466, NGC 5897, NGC 6397 and NGC 6809, we find that our results are broadly consistent with the literature. In particular, considering the systematic error, the results derived

by the KDE are consistent with the previous results in Table 2, which are obtained by the method of Nataf et al. (2013) and the analysis of the differential luminosity function and the cumulative luminosity function adopted by Fusi Pecci et al. (1990), Sarajedini (1992) and Ferraro et al. (1999). The KDE method is very convenient for finding the RGB bump feature.

In NGC 6656, Nataf et al. (2013) presented that the RGB bump magnitude in $V$ is $13.974 \pm 0.013$. Lee (2015) presented that a distinctive RGB split due to the different metal abundances in M22. The two populations of the RGB show the calcium-weak (Ca-w) group and the calcium-strong (Ca-s) group, respectively. They obtained $V_{bump} = 13.91$ mag for the Ca-w group while $V_{bump} = 14.06$ mag for the Ca-s group. They found that the difference in the RGB bump magnitude between two populations of the RGB is due to the difference in metallicity. They also obtained that the mean RGB bump magnitude of the metal-rich population (Ca-s group) is fainter than that of the metal-poor population (Ca-w group). Considering the systematic error, the RGBB magnitude derived by the KDE is $13.936 \pm 0.030$ mag. It matches the results presented by Nataf et al. (2013) and Lee (2015). In the cluster, the parameter space of $V_{B,M}$ in the log-likelihood function ranges from $V_{B,K} - 0.5$ to $V_{B,K} + 0.5$. The RGBB magnitude calculated by the maximum-likelihood analysis is 13.75 mag. The width of the RGBB ranges from $13.75 - 3\sigma_{B,V}$ (13.483) mag to $13.75 + 3\sigma_{B,V}$ (14.017) mag.

## 4 The metallicity-$M_V$ relation for metal-poor globular clusters

[M/H] shows the global metallicity of globular clusters. It is defined as (Valcarce et al. 2012)

$$[\mathrm{M/H}] = \log(Z/X) - \log(Z/X)_{sun} \tag{12}$$

$Z$ and $Z_{sun}$ represent the metal mass abundance of the cluster and the metal mass abundance of the Sun. $X$ and $X_{sun}$ represent the mass abundance of hydrogen of the cluster and the mass abundance of hydrogen of the Sun. The metallicity abundance [Fe/H] of 7 GGCs was obtained from Carretta et al. (2009). The global metallicity [M/H] is computed using the [Fe/H]-[M/H] relation presented by Salaris et al. (1993) and Carretta et al. (2009):

$$[\mathrm{M/H}] = [\mathrm{Fe/H}] + \log(0.638 * 10^{[\alpha/\mathrm{Fe}]} + 0.362) \tag{13}$$

[$\alpha$/Fe] is obtained from the literature (McWilliam et al. 1992; Carney 1996; Johnson et al. 2009; Koch and McWilliam 2011, 2014; Khamidullina et al. 2014; Boberg et al. 2015; Kamann et al. 2016; Johnson et al. 2017; Rain et al. 2019).

The RGBB absolute magnitude $M_V$ is calculated using the following relation:

$$M_V = V_{RGBB} - (m - M)_V \tag{14}$$

The apparent distance modulus $(m - M)_V$ is obtained from the literature (Bellazzini et al. 2004; Harris 2010; Kunder et al. 2013; Kaluzny et al. 2014; Kains et al. 2015). $V_{RGBB}$ is the RGBB brightness derived by the maximum-likelihood function analysis. The global metallicity-$M_V$ relation is shown in Fig. 3. Red pluses represent the RGBB brightnesses derived in the present analysis. Blue crosses show the RGBB brightnesses presented by Nataf et al. Black squares present the RGBB brightnesses of NGC 5694, NGC 6287 and NGC 6293 obtained by Zoccali et al.

Based on the RGBB brightnesses of 25 metal-poor globular clusters except for NGC 6287 and NGC 6293, the empirical relation between [M/H] and $M_V$ for metal-poor GGCs is obtained by the linear fit:

$$M_V = 0.56 * [\mathrm{M/H}] + 1.18 \tag{15}$$

## 5 Comparison between observed RGBB absolute magnitudes and predicted RGBB absolute magnitudes

Many studies try to explain discrepancies in the RGBB brightness between theory and observation through different stellar models (Riello et al. 2003; Di Cecco et al. 2010; Joyce and Chaboyer 2015). Investigations (Di Cecco et al. 2010; Joyce and Chaboyer 2015; Dotter et al. 2017; Joyce and Chaboyer 2018) pointed out that a proper inclusion of the $\alpha$-element enhancement and diffusion in models will affect the RGB bump brightness and help in reducing the magnitude difference between predicted RGBB magnitudes and observed RGBB magnitudes. Di Cecco et al. (2010) found that discrepancies in the RGBB brightness for globular clusters with $[\mathrm{M/H}] \leqslant -1.6$ remain even if they considered $\alpha$-enhanced, CNO-enhanced and helium-enhanced phenomena in their models. Joyce and Chaboyer (2015) also presented that discrepancies in the RGBB brightnesses for globular clusters with $[\mathrm{Fe/H}] \leqslant -1.5$ remain when they considered $\alpha$-enhanced phenomenon in DSEP models. The metallicity abundances [Fe/H] of 7 samples in our work are all smaller than $-1.6$. The global metallicity abundances [M/H] of 7 samples in our work are all smaller than $-1.4$. We try to verify discrepancies in the RGBB brightness for samples of globular clusters with $[\mathrm{M/H}] \leqslant -1.4$ by using the BASTI models (Cordier et al. 2007; Hidalgo et al. 2018; Pietrinferni et al. 2021).

The solar-scaled BASTI model (Pietrinferni et al. 2004; Cordier et al. 2007) are updated based on previous models (Cassisi and Salaris 1997). The detailed equation of state

by A.W. Irwin[1] has been used. A brief discussion of its main characteristics can be found in (Cassisi et al. 2003). The radiative opacities are from the OPAL tables (Iglesias and Rogers 1996) for temperatures larger than 10000 K, whereas the opacities by Alexander and Ferguson (1994) have been adopted for lower temperatures. The nuclear reaction rates have been updated by using values from the NACRE database (Angulo et al. 1999) and the determination by Kunz et al. (2002). Many other informations can be found in Pietrinferni et al. (2004). The $\alpha$-enhanced BASTI model (Pietrinferni et al. 2006; Cordier et al. 2007) are updated based on the consideration of the new chemical and physical inputs for the $\alpha$-enhanced library. The $\alpha$-enhanced distribution has been used in the nuclear network, the radiative opacity (Iglesias and Rogers 1996; Alexander and Ferguson 1994) and conductive opacity (Potekhin et al. 1999), and the equation of state (EOS). We adopt canonical models (Pietrinferni et al. 2004, 2006) without overshooting, gravitational settling, radiative acceleration, convective overshooting, rotational mixing, atomic diffusion of helium and heavy elements. The models both consider the mass loss presented by Reimers (1975).

In Fig. 3, a comparison between theory and observation is shown. Red pluses, green pluses, blue crosses and black squares in Fig. 3 represent the observational RGBB absolute magnitude $M_V$. The black full line shows the linear relation between [M/H] and $M_V$ for metal-poor GGCs (presented in equation (15)). The black full line is obtained by linear fitting. The other four lines represent theoretical relations between [M/H] and RGBB absolute magnitude $M_V$ calculated by the $\alpha$-enhanced BaSTI models (Pietrinferni et al. 2006) and the standard solar-scaled BaSTI models (Pietrinferni et al. 2004). The purple full line and the purple dashed line respectively represent theoretical lines with 13.8 Gyr calculated by the standard solar-scaled models and the $\alpha$-enhanced models. The red full line and the red dashed line represent theoretical lines with 10 Gyr calculated by the solar-scaled models and the $\alpha$-enhanced models.

Obviously, the predicted RGB bump luminosities by the $\alpha$-enhanced models are fainter than the predicted RGB bump luminosities with same age by the solar-scaled models. The magnitude difference between the predicted RGBB luminosities by the solar-scaled models and the observed RGBB luminosities are much larger than the magnitude difference between the predicted RGBB luminosities with same age by the $\alpha$-enhanced models and the observed RGBB luminosities. Comparing the black full line with the other four lines predicted by BASTI models, we find that the observed RGBB luminosities are fainter than the predicted RGBB luminosities presented by BASTI models. No

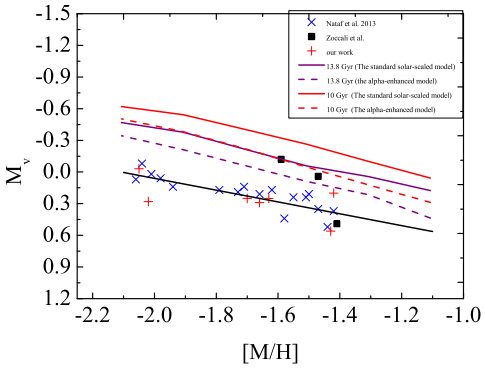


**Fig. 3** The absolute magnitude of RGBB $M_V$ is shown as a function of [M/H]. Absolute magnitudes of RGBB of 7 GGCs in our work are plotted by red pluses. Observations of Zoccali et al. are plotted by black squares. Blue crosses present observations of Nataf et al. The theoretical relations between [M/H] and $M_V$ calculated by the standard solar-scaled model are shown by the purple full line with 13.8 Gyr and the red full line with 10 Gyr. The theoretical relations calculated by the alpha-enhanced model are shown by the purple dashed line with 13.8 Gyr and the red dashed line with 10 Gyr. The black full line shows the empirical relation between [M/H] and $M_V$ for metal-poor GGCs obtained by the linear fit

consideration of other errors in the observed RGBB brightnesses, the result coincides with other conclusions presented by Di Cecco et al. (2010) and Joyce and Chaboyer (2015).

## 6 Discussions and conclusions

Many studies (Di Cecco et al. 2010; Cassisi et al. 2011; Joyce and Chaboyer 2015; Song et al. 2018) found a discrepancy between predicted RGBB brightness and observational RGBB brightness, especially for metal-poor globular clusters. The detection of RGBB brightness in metal-poor globular clusters is helpfull because this region of the HR diagram reflects an evolutionary sequence that is highly sensitive to the physics assumed in stellar models. We use the new observational data (*Gaia* DR2) to analyse the RGBB brightnesses of 7 metal-poor galactic globular clusters. Seven metal-poor globular clusters are revisited.

In our work, three methods (the differential luminosity function, the maximum-likelihood analysis via MCMC, kernel density estimation) are used to find the RGBB feature in the metal-poor GGCs. These results derived by the DLF, maximum-likelihood analysis and KDE are consistent with previous results listed in Table 2. Due to its effectiveness and flexibility, kernel density estimation has become a significant tool to estimate the continuous density function. It is a nonparametric method. Based on the magnitude distribution of the RGB stars, the overdensity position is found. It directly reflects the density distribution according to observational data. Based on the results presented by KDE, the maximum-likelihood analysis via MCMC can obtain the accurate RGBB brightness in the specified parameter space.

[1] A full description of this EOS can be found at http://freeeos.sourceforge.net.

The width of the RGB bump is also presented. Finally, the relation between global metallicity [M/H] and $M_V$ is obtained for galactic globular clusters with [M/H] $\leq -1.4$.

In Fig. 3, a comparison between BASTI models and the observed RGBB brightness from our work and other studies is carried out. We verify that the discrepancy between observations and theory exists for metal-poor globular clusters with [M/H] $\leq -1.4$.

In conclusion, we present the RGB bump magnitudes in $G$ band and $V$ band for 7 galactic globular clusters with [M/H] $\leq -1.4$. A novel statistical approach KDE is used to find the RGB bump magnitudes of samples. Compared with previous results listed in Table 2, we find that the RGB bump magnitudes of GCs obtained by the maximum-likelihood analysis and KDE match with them as we consider the systematic error on the conversion between G band and V band. We use the $\alpha$-enhanced BaSTI models and the solar-scaled models to verify the discrepancy between observations and theory for GGCs with [M/H] $\leq -1.4$.

In the future, it would be interesting to apply the KDE technique to all of the globular clusters presented in Nataf et al.'s sample.

**Acknowledgements** This work was partially funded by the NSFC of China (Grant Nos. 11333006, 11521303, 11373020, 11503079, 11603009, 11503076, 11503079, 11773064, 11803009, 11863003, and 12073069) and the foundation of the Chinese Academy of Sciences (Grant No. XDB09010202). This work was partially supported by the Natural Science Foundation of Fujian Province under grant Nos. 2016J05013, Nos. 2018J05006 and Nos. 2018J05007, the Education Department of Fujian Province JAT200272, the Key Laboratory for the Structure and Evolution of Celestial Objects, Chinese Academy of Sciences (Grant No. OP201404 and B615015), the Yunnan Natural Science Foundation (No. 2019FB008) and Yunnan Applied Basic Research Projects (grant No. 2017B008) and the Science Foundation of Jimei University (Grant No. C613030 and No. C519141(ZP2020060)). This work has made use of data from the European Space Agency (ESA) mission *Gaia* (https://www.cosmos.esa.int/gaia), processed by the *Gaia* Data Processing and Analysis Consortium (DPAC, https://www.cosmos.esa.int/web/gaia/dpac/consortium). Funding for the DPAC has been provided by national institutions, in particular, institutions participating in the *Gaia* Multilateral Agreement. F. Song also gratefully acknowledges the computing time granted by the Yunnan Observatories, and provided on the facilities at the Yunnan Observatories Supercomputing Platform.

## References

Alexander, D.R., Ferguson, J.W.: Astrophys. J. **437**, 879 (1994). https://doi.org/10.1086/175039

Alves, D.R., Sarajedini, A.: Astrophys. J. **511**, 225 (1999). https://doi.org/10.1086/306655

Angulo, C., Arnould, M., Rayet, M., et al.: Nucl. Phys. A **656**, 3 (1999). https://doi.org/10.1016/S0375-9474(99)00030-5

Bellazzini, M., Ferraro, F.R., Sollima, A., et al.: Astron. Astrophys. **424**, 199 (2004). https://doi.org/10.1051/0004-6361:20035910

Bjork, S.R., Chaboyer, B.: Astrophys. J. **641**, 1102 (2006). https://doi.org/10.1086/500505

Boberg, O.M., Friel, E.D., Vesperini, E.: Astrophys. J. **804**, 109 (2015). https://doi.org/10.1088/0004-637X/804/2/109

Bono, G., Cassisi, S., Zoccali, M., et al.: Astrophys. J. Lett. **546**, L109 (2001). https://doi.org/10.1086/318866

Botev, Z.I., Grotowski, J.F., Kroese, D.P.: Ann. Stat. **38**(5), 2916–2957 (2010)

Carney, B.W.: Publ. Astron. Soc. Pac. **108**, 900 (1996). https://doi.org/10.1086/133811

Carrasco, J.M., Evans, D.W., Montegriffo, P., et al.: Astron. Astrophys. **595**, A7 (2016). https://doi.org/10.1051/0004-6361/201629235

Carretta, E., Bragaglia, A., Gratton, R., et al.: Astron. Astrophys. **508**, 695 (2009). https://doi.org/10.1051/0004-6361/200913003

Cassisi, S., Salaris, M.: Mon. Not. R. Astron. Soc. **285**, 593 (1997). https://doi.org/10.1093/mnras/285.3.593

Cassisi, S., Salaris, M., Bono, G.: Astrophys. J. **565**, 1231 (2002). https://doi.org/10.1086/324695

Cassisi, S., Salaris, M., Irwin, A.W.: Astrophys. J. **588**, 862 (2003). https://doi.org/10.1086/374218

Cassisi, S., Marín-Franch, A., Salaris, M., et al.: Astron. Astrophys. **527**, A59 (2011). https://doi.org/10.1051/0004-6361/201016066

Cohen, R.E., Hempel, M., Mauro, F., et al.: Astron. J. **150**, 176 (2015). https://doi.org/10.1088/0004-6256/150/6/176

Cordier, D., Pietrinferni, A., Cassisi, S., et al.: Astron. J. **133**, 468 (2007). https://doi.org/10.1086/509870

Di Cecco, A., Bono, G., Stetson, P.B., et al.: Astrophys. J. **712**, 527 (2010). https://doi.org/10.1088/0004-637X/712/1/527

Dotter, A., Conroy, C., Cargile, P., et al.: Astrophys. J. **840**, 99 (2017). https://doi.org/10.3847/1538-4357/aa6d10

Evans, D.W., Riello, M., De Angeli, F., et al.: Astron. Astrophys. **616**, A4 (2018). https://doi.org/10.1051/0004-6361/201832756

Fekadu, N., Sandquist, E.L., Bolte, M.: Astrophys. J. **663**, 277 (2007). https://doi.org/10.1086/518637

Ferraro, F.R., Messineo, M., Fusi Pecci, F., et al.: Astron. J. **118**, 1738 (1999). https://doi.org/10.1086/301029

Fusi Pecci, F., Ferraro, F.R., Crocker, D.A., et al.: Astron. Astrophys. **238**, 95 (1990)

Gaia Collaboration, Brown, A.G.A., Vallenari, A., et al.: Astron. Astrophys. **616**, A1 (2018b). https://doi.org/10.1051/0004-6361/201833051

Gaia Collaboration, Helmi, A., van Leeuwen, F., et al.: Astron. Astrophys. **616**, A12 (2018d). https://doi.org/10.1051/0004-6361/201832698

Gaia Collaboration, Prusti, T., de Bruijne, J.H.J., et al.: Astron. Astrophys. **595**, A1 (2016). https://doi.org/10.1051/0004-6361/201629272

Gramacki, A.: Nonparametric Kernel Density Estimation and Its Computational Aspects. Springer, Berlin (2018)

Harris, W.E.: (2010). arXiv:1012.3224

Hatfield, P.W., Lindsay, S.N., Jarvis, M.J., et al.: Mon. Not. R. Astron. Soc. **459**, 2618 (2016). https://doi.org/10.1093/mnras/stw769

Hidalgo, S.L., Pietrinferni, A., Cassisi, S., et al.: Astrophys. J. **856**, 125 (2018). https://doi.org/10.3847/1538-4357/aab158

Iglesias, C.A., Rogers, F.J.: Astrophys. J. **464**, 943 (1996). https://doi.org/10.1086/177381

Johnson, C.I., Pilachowski, C.A., Michael Rich, R., et al.: Astrophys. J. **698**, 2048 (2009). https://doi.org/10.1088/0004-637X/698/2/2048

Johnson, C.I., Caldwell, N., Rich, R.M., et al.: Astrophys. J. **836**, 168 (2017). https://doi.org/10.3847/1538-4357/836/2/168

Joyce, M., Chaboyer, B.: Astrophys. J. **814**, 142 (2015). https://doi.org/10.1088/0004-637X/814/2/142

Joyce, M., Chaboyer, B.: Astrophys. J. **856**, 10 (2018). https://doi.org/10.3847/1538-4357/aab200

Kains, N., Arellano Ferro, A., Figuera Jaimes, R., et al.: Astron. Astrophys. **578**, A128 (2015). https://doi.org/10.1051/0004-6361/201424600

Kaluzny, J., Thompson, I.B., Dotter, A., et al.: Acta Astron. **64**, 11 (2014)
Kamann, S., Husser, T.-O., Brinchmann, J., et al.: Astron. Astrophys. **588**, A149 (2016). https://doi.org/10.1051/0004-6361/201527065
Khamidullina, D.A., Sharina, M.E., Shimansky, V.V., et al.: Astrophys. Bull. **69**, 409 (2014). https://doi.org/10.1134/S199034131404004X
King, C.R., Da Costa, G.S., Demarque, P.: Astrophys. J. **299**, 674 (1985). https://doi.org/10.1086/163733
Koch, A., McWilliam, A.: Astron. J. **142**, 63 (2011). https://doi.org/10.1088/0004-6256/142/2/63
Koch, A., McWilliam, A.: Astron. Astrophys. **565**, A23 (2014). https://doi.org/10.1051/0004-6361/201323119
Kunder, A., Stetson, P.B., Cassisi, S., et al.: Astron. J. **146**, 119 (2013). https://doi.org/10.1088/0004-6256/146/5/119
Kunz, R., Fey, M., Jaeger, M., et al.: Astrophys. J. **567**, 643 (2002). https://doi.org/10.1086/338384
Landolt, A.U.: Astron. J. **137**, 4186 (2009). https://doi.org/10.1088/0004-6256/137/5/4186
Lee, J.-W.: Astrophys. J. Suppl. Ser. **219**, 7 (2015). https://doi.org/10.1088/0067-0049/219/1/7
Lewis, A., Bridle, S.: Phys. Rev. D **66**, 103511 (2002). https://doi.org/10.1103/PhysRevD.66.103511
McWilliam, A., Geisler, D., Rich, R.M.: Publ. Astron. Soc. Pac. **104**, 1193 (1992). https://doi.org/10.1086/133108
Nataf, D.M.: Mon. Not. R. Astron. Soc. **445**, 3839 (2014). https://doi.org/10.1093/mnras/stu1974
Nataf, D.M., Gould, A.P., Pinsonneault, M.H., et al.: Astrophys. J. **766**, 77 (2013). https://doi.org/10.1088/0004-637X/766/2/77
Pancino, E., Ferraro, F.R., Bellazzini, M., et al.: Astrophys. J. Lett. **534**, L83 (2000). https://doi.org/10.1086/312658
Perren, G.I., Giorgi, E.E., Moitinho, A., et al.: Astron. Astrophys. **637**, A95 (2020). https://doi.org/10.1051/0004-6361/201937141
Pietrinferni, A., Cassisi, S., Salaris, M., et al.: Astrophys. J. **612**, 168 (2004). https://doi.org/10.1086/422498
Pietrinferni, A., Cassisi, S., Salaris, M., et al.: Astrophys. J. **642**, 797 (2006). https://doi.org/10.1086/501344
Pietrinferni, A., Hidalgo, S., Cassisi, S., et al.: Astrophys. J. **908**, 102 (2021). https://doi.org/10.3847/1538-4357/abd4d5
Piotto, G., King, I.R., Djorgovski, S.G., et al.: Astron. Astrophys. **391**, 945 (2002). https://doi.org/10.1051/0004-6361:20020820
Piotto, G., Milone, A.P., Bedin, L.R., et al.: Astron. J. **149**, 91 (2015). https://doi.org/10.1088/0004-6256/149/3/91
Potekhin, A.Y., Chabrier, G., Shibanov, Y.A.: Phys. Rev. E **60**, 2193 (1999)
Rain, M.J., Villanova, S., Munõz, C., et al.: Mon. Not. R. Astron. Soc. **483**, 1674 (2019). https://doi.org/10.1093/mnras/sty3208
Reimers, D.: Mem. Soc. R. Sci. Liege **8**, 369 (1975)
Riello, M., Cassisi, S., Piotto, G., et al.: Astron. Astrophys. **410**, 553 (2003). https://doi.org/10.1051/0004-6361:20031272
Salaris, M., Chieffi, A., Straniero, O.: Astrophys. J. **414**, 580 (1993). https://doi.org/10.1086/173105
Sarajedini, A.: Astron. J. **104**, 178 (1992). https://doi.org/10.1086/116229
Sarajedini, A., Bedin, L.R., Chaboyer, B., et al.: Astron. J. **133**, 1658 (2007). https://doi.org/10.1086/511979
Sollima, A., Ferraro, F.R., Pancino, E., et al.: Mon. Not. R. Astron. Soc. **357**, 265 (2005). https://doi.org/10.1111/j.1365-2966.2005.08646.x
Song, F., Li, Y., Wu, T., et al.: Astrophys. J. **869**, 109 (2018). https://doi.org/10.3847/1538-4357/aaecd3
Valcarce, A.A.R., Catelan, M., Sweigart, A.V.: Astron. Astrophys. **547**, A5 (2012). https://doi.org/10.1051/0004-6361/201219510
Yuan, Z., Wang, J., Zhou, M., et al.: Astrophys. J. **820**, 65 (2016). https://doi.org/10.3847/0004-637X/820/1/65
Yuan, Z., Wang, J., Worrall, D.M., et al.: Astrophys. J. Suppl. Ser. **239**, 33 (2018). https://doi.org/10.3847/1538-4365/aaed3b
Yuan, Z., Jarvis, M.J., Wang, J.: Astrophys. J. Suppl. Ser. **248**, 1 (2020). https://doi.org/10.3847/1538-4365/ab855b
Zoccali, M., Cassisi, S., Piotto, G., et al.: Astrophys. J. Lett. **518**, L49 (1999). https://doi.org/10.1086/312064

**Publisher's Note** Springer Nature remains neutral with regard to jurisdictional claims in published maps and institutional affiliations.